Applied Surface Science 496 (2019) 143735

Contents lists available at ScienceDirect

Applied Surface Science

journal homepage: www.elsevier.com/locate/apsusc

Full length article

Highly porous carbon films fabricated by magnetron plasma enhanced chemical vapor deposition: Structure, properties and implementation

O.M. Slobodian[a,*], A.V. Rusavsky[a], A.V. Vasin[a,b], O.Yu. Khyzhun[c], O.I. Gudymenko[a], V.P. Kladko[a], A.S. Nikolenko[a], B.I. Tsykaniuk[a], P.M. Lytvyn[a], Yu.V. Gomeniuk[a], O.M. Fesenko[d], A.N. Nazarov[a,b]

[a] Lashkaryov Institute of Semiconductor Physics NAS of Ukraine, 41 pr. Nauki, 03028 Kyiv, Ukraine
[b] National Technical University of Ukraine "Igor Sikorsky KPI", 37 pr. Peremohy, 03056 Kyiv, Ukraine
[c] Frantsevych Institute for Problems of Materials Science NAS of Ukraine, 3 str. Krzhizhanovsky, 03142 Kyiv, Ukraine
[d] Institute of Physics NAS of Ukraine, 46 av. Nauki, 03028 Kyiv, Ukraine

A B S T R A C T

The new method is suggested of formation of highly porous graphite-like thin films by radio frequency magnetron plasma enhanced chemical vapor deposition from argon-methane gas mixture. The prepared films were characterized before and after thermal annealing by XPS, XES, FTIR, Raman spectroscopy, XRD, XRR, AFM, and electrical measurements. Deconvolution of XPS spectra has demonstrated a significant growth of sp^2/sp^3 ratio from 1 for as-deposited films to 12 for the films annealed at 650 °C for 5 min. FTIR spectra have confirmed that thermal annealing results in reduction of H– and OH– functional groups and formation of C=C bonds. The analysis of Raman spectra has shown that the annealing incorporates additional defects in graphite plane. XRD has shown that films are amorphous. Estimation of porosity from XRR measurements gave values of about 59% for as-deposited films and 34% for annealed films. AFM has shown that roughness of the films decreases from 3.3 to 0.6 nm during treatment at 650 °C in inert atmosphere. The size of pores was found to be few tens of nanometers. The electrical measurements have shown that after annealing the resistivity decreases by up to 5 orders of magnitude. Annealed films have demonstrated perceptible sensitivity to ammonia and water vapor.

1. Introduction

Carbon-based films, which possess unique properties due to tunability of their chemical bonds, have been widely studied in recent decades [1–3]. Physical and electrical properties of these materials are determined by the chemical structure, relative ratio of sp^2 to sp^3 bonds as well as by growth morphology. Nanoscale porosity is a morphological parameter closely related to electrical properties of the material and to its sensitivity to chemical environment. Nanoporous carbon (np-C) film is a very attractive material for different fields of applications such as catalysis [4], energy storage [5], purification of gases and liquids [6,7] and chemical gas sensors [8]. It is well known, that np-C films with average pore diameter about 1 nm can be fabricated by different deposition techniques including chemical vapor deposition [9], magnetron sputtering [10], pulsed layer deposition [11], spray coating [12] and ultrasonic deposition [13]. For many applications porous carbon film has to be conductive, for example, in biomedical electronic devices and chemical sensors based on the electrical resistance response. Combination of porosity and conductivity in such films is a great advantage but it is a big challenge as well. High conductivity in carbon is, first of all, associated with high concentration of sp^2 bonds and highly percolated graphitic/graphenic phases.

Recently we have studied the effects of magnetron deposition conditions and consequent thermal treatments on structural, morphological and electrical properties of amorphous carbon-rich silicon-carbon alloy films [14,15]. It was demonstrated that the density of the a-SiC:H films deposited by magnetron sputtering can be varied by discharge power and methane incorporation. In the present work we demonstrate an original method of "magnetron plasma enhanced chemical vapor deposition" of low density amorphous carbon. It will be shown that poor conductivity and chemical sensitivity of as-deposited films can be strongly enhanced by thermal annealing.

2. Experimental details

2.1. Sample preparation

Deposition of low-density amorphous carbon films was performed using specific deposition regime of typical planar radio frequency magnetron with silicon target (160 cm diameter). At first deposition

* Corresponding author.
E-mail address: akapulko20@gmail.com (O.M. Slobodian).

https://doi.org/10.1016/j.apsusc.2019.143735
Received 7 May 2019; Received in revised form 11 August 2019; Accepted 19 August 2019
Available online 20 August 2019
0169-4332/

stage a very thin “adhesion” layer (few nanometers) was deposited on the substrate using pure argon at pressure 0.8 Pa and discharge power 200 W. After “adhesion” layer is formed the deposition process was modified by reducing of discharge power down to 60–80 W, and introducing of methane that resulted in the increase of the pressure up to 1.0 Pa. At such parameters no silicon sputtering occurred on the silicon target and the deposition process is determined primarily by plasma enhanced decomposition of methane in the near-substrate region. Methane is commonly used for plasma enhanced chemical vapor deposition (PECVD) of amorphous hydrogenated carbon films [16]). It is quite “technological” and easily accessible gas. The above described deposition mode is somewhat similar to “low power/pressure” plasma enhanced chemical vapor deposition (PECVD) process and can be denoted as “magnetron PECVD”. The adhesion silicon-rich layer provides sufficient durability of the interface between a substrate (silicon, silicon oxide) and very soft carbon film to make possible further contact processing and experiments. Si(100) wafers and Si wafers with 200 nm silicon oxide layer grown by thermal oxidation were used as substrates. Substrate holder was heated up to 200 °C before plasma ignition for surface cleaning and improvement of the adhesion, but no intentional heating was used during the deposition process.

Deposited a-C:H films were modified by thermal annealing for enhancement of electrical conductivity. “Graphitization” has been performed by thermal annealing in N_2 atmosphere at temperatures up to 650 °C for 5 min. Higher annealing temperature was not used due to combustion of carbon by residual oxygen contaminations in the chamber. All discussed results are related to four kinds of the carbon film deposited using different values of discharge power, methane flow rate and time of deposition (see Table 1).

2.2. Characterization

The chemical composition of as-deposited films was examined by X-ray photoelectron spectroscopy (XPS). The XPS spectra were recorded using excitation by an X-ray Mg Kα source (E = 1253.6 eV). Additionally, X-ray emission spectroscopy (XES) was used to record the C—K XES band giving information on the energy distribution of C 2p states. The C—K spectra had been recorded with an RSM-500 spectrometer-monochromator equipped with a diffraction grating (600 groves/mm, radius of curvature of about 6 m). It is worth mentioning that the XPS spectra are very sensitive to surface charging due to charge loss through electron emission [17]. XPS spectra are often corrected using C 1s core-level spectrum as a reference line to account for charging effects [18,19]. This approach is not applicable for carbon films. Therefore, a flood gun was used in the present XPS experiments to overcome charging effects as it is suggested to do in such a case. The XES technique is not sensitive to charging effects [20].

Investigation of molecular bonds in as-deposited and annealed samples was performed also by Fourier-transform infrared (FTIR) spectroscopy using Bruker Vertex 70 V spectrometer. The micro-Raman analysis have been performed by inVia micro-Raman spectrometer (Renishaw, UK) using a laser with 633-nm wavelength and spot size of 10 μm. The laser power on the sample surface was always kept below 1 mW to avoid laser induced damages.

The structure of the carbon films was estimated by X-ray diffraction (XRD) technique using PANalytical X'Pert Pro MRD XL diffractometer with CuKα1 radiation (0.15405 nm). No diffraction peaks were observed in diffractograms proving that the films are amorphous. Another technique, X-ray reflectivity (XRR), was used to determine a density and thickness of the films.

Surface morphology was studied by atomic force microscopy (AFM) with NanoScope IIIa Dimension 3000 (USA).

Four point probe method and transmittance line (TSL) technique [21] were used for the analysis of electrical properties. The gas sensitivity was examined by measurement of resistance between Ni contacts (distance between the contacts is 288 μm). Measurements were performed with semiconductor parameter analyzer Agilent 4156C (USA).

Table 1
Sample labels and corresponding deposition conditions.

Sample	Working gas, (Ar/CH_4), sccm	Power, W	Deposition time, min
#1	14/6.0	70	10
#2	15/4.1	60	18
#3	14/6.0	85	30
#4	15/4.1	63	40

3. Chemical analysis

3.1. XPS and XES

The survey XPS spectra are presented in Fig. 1(a). A significant amount of oxygen is detected (Table 2). However, as can be seen from Fig. 1(c), the maxima of the O 1s core-level spectra in all samples are located at about 532.5 eV that corresponds rather to oxygen-containing atmospheric species adsorbed in the carbon films [22]. Furthermore, the as-deposited sample #2 contains minor nitrogen contamination (8.4 at.%, Table 2), that disappeared after annealing (see Fig. 1(a)). As can be seen from data listed in Table 2, the annealing of the both films causes decreasing the content of oxygen on their surfaces by about 30%.

Fig. 1(b) presents the high resolution XPS C 1s core-level spectra of the carbon films. As-deposited films reveal the C 1s spectra with their maxima at about 285.0 eV, which is close to the C 1s binding energy of diamond [23]. Annealing at 650 °C results in the C 1s spectra shift at about 284.4 eV that well corresponds to that of the C 1s spectrum in graphite [24]. Furthermore, the annealed carbon films reveal the enhanced intensity of the spectra in the higher energy slope of the peak. This peculiarity is mostly due to the π shake-up satellite, which is characteristic for the C 1s spectra of graphite and conjugated organic compounds [25,26], but is not observed in diamond [27]. The above XPS data allow suggesting that as-deposited carbon films are characterized by C—C bonds with dominant sp^3 hybridization, while annealing lead to transformation of four-fold coordination into three-fold coordination with dominant sp^2 hybridization that is in a good agreement with [28–30].

Deconvolution of C 1s spectra for as-deposited and post annealed films is presented in Fig. 1(d). Spectra were fitted by three components originated from sp^3- and sp^2-coordinated carbon-carbon bonds with minor contribution from carbon-oxygen bonds. Binding energy for sp^2 carbon was fixed at 284.4 eV, and that for sp^3 — at 285.2 eV. The fitting procedure clearly demonstrates that concentration of sp^2 hybridized carbon bonds increases after thermal treatment. The annealed sample has 77% of sp^2 and 6.2% of sp^3 carbon bonds as compared to 40.9% of sp^2 and 43.4% of sp^3 in as-deposited film. The peak, responsible for C—O bonds (286.6 eV) is weakly affected by annealing.

To prove the suggestion about transformation of the sp^3 hybridized carbon films to sp^2 hybridized films after annealing at 650 °C, the C Kα XES band of the as-deposited and post annealed carbon films have been analyzed (Fig. 2). For comparison, the C Kα band of graphite is also plotted in this figure. It is evident that the shapes of the C Kα XES bands are very similar in both as-deposited carbon films. The fine structure of C Kα XES bands in these samples is similar to that observed in diamond and carbon materials possessing C—C bonds with sp^3 hybridization [31].

It is known that the high-energy part of the C Kα band of graphite is formed by C 2p states involved in the π-bonding states (peculiarity ‘e’, Fig. 2), while the peculiarities ‘c’ and ‘d’ of the C Kα spectra are due to contributions of the C 2p states involved in the π + σ-bonding [14,15]. As can be seen from Fig. 2, the C Kα bands of the as-deposited carbon films reveal almost complete absence of the feature ‘e’ inherent to the pure π-bonding C 2p states that can be interpreted as an evidence of

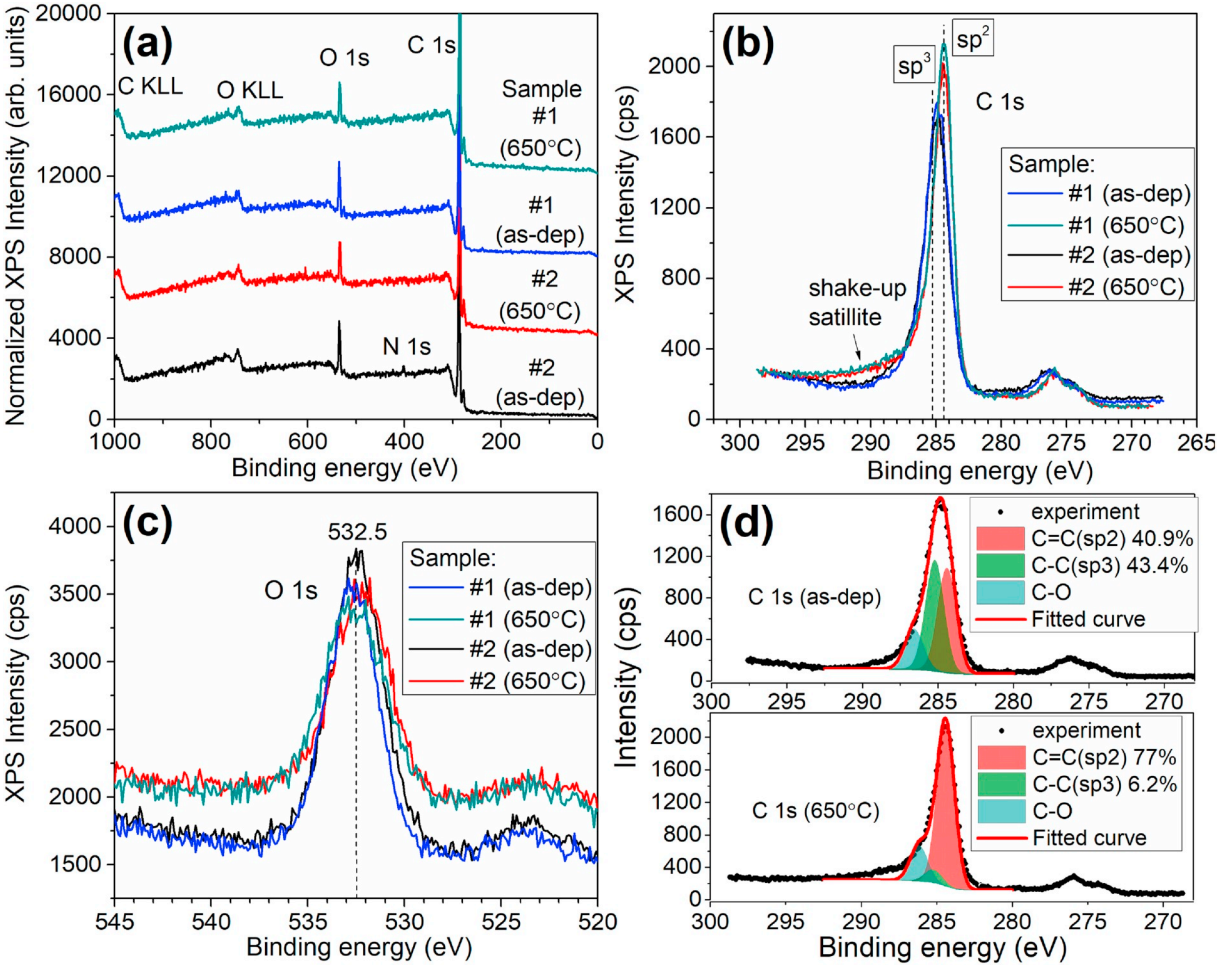

Fig. 1. XPS data obtained for the porous carbon films. (a) — Survey spectra of two samples (#1 and #2), (b) — C 1s core-level spectra and (c) — O 1s core-level spectra for both as-deposited and annealed at 650 °C films. (d) — Deconvolution of C 1s spectra for sample #1 before and after annealing at 650 °C.

Table 2
Composition (at.%) of the film surfaces as determined by the present XPS measurements.

Carbon film	C	O	N
#1 (as-dep)	68.6	31.4	–
#1 (650 °C)	78.7	21.3	–
#2 (as-dep)	59.5	32.1	8.4
#2 (650 °C)	76.5	23.5	–

dominant sp^3 coordination [31,32]. After annealing, the films demonstrate the C Kα bands possessing well-resolved feature 'e' indicating π-bonding C 2p states that is in a good agreement with XPS data.

3.2. FTIR

Fig. 3 illustrates FTIR spectra of as-deposited and annealed samples. Spectra of as-deposited samples exhibited dominant adsorption multiplete at 2700–3000 cm^{-1} attributed to stretching vibration modes of C(sp^3)—H bonds [33]. Minor bands at 1110 cm^{-1} and 1420 cm^{-1} are originated presumably from carboxyl COOH and hydroxyl groups attached to carbon atoms C—OH [28,34,35] while a prominent band around 1700 cm^{-1} and a broad band in the range of 3000–3500 cm^{-1} is unambiguously related to carbonyl C═O bonds and hydroxyl groups in adsorbed water (Fig. 3(a)). Presence of such bonds in our carbon material is typical for amorphous hydrogenated carbon films (a-C:H) [36].

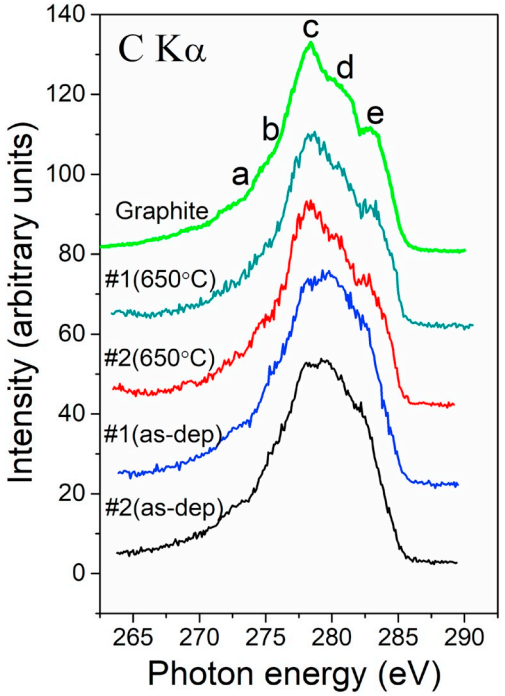

Fig. 2. XES spectra of as-deposited and annealed at 650 °C samples #1 and #2, and C Kα band of graphite.

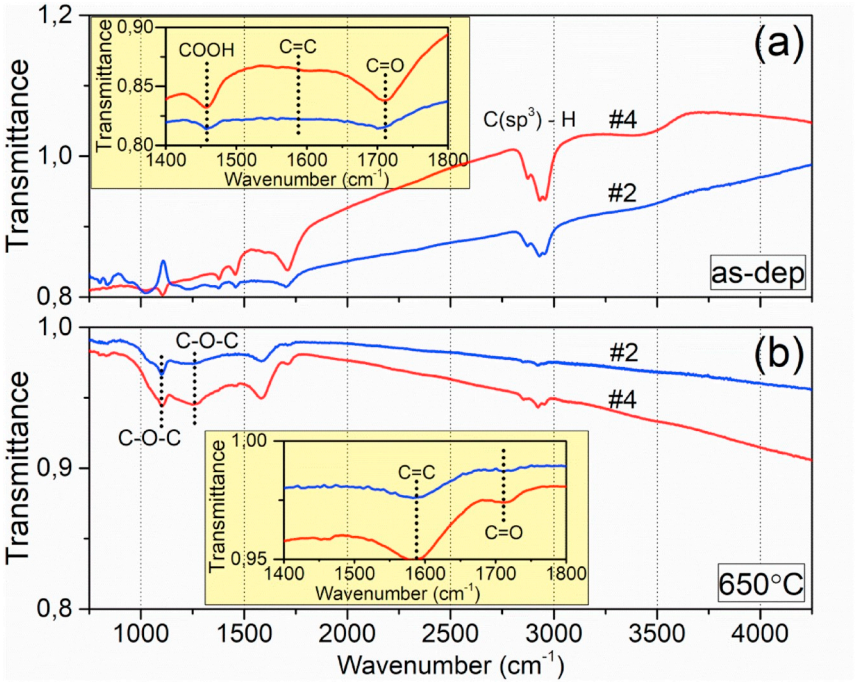

Fig. 3. FTIR spectra of carbon films (samples #2 and #4) (a) before and (b) after thermal annealing at 650 °C.

Thermal annealing at 650 °C results in reduction of H- and OH-related adsorption bands. At the same time, the new prominent peak with maximum at 1600 cm^{-1} is now detected, that indicates formation of C=C bonds (Fig. 3(b)) [34]. Another evident result of annealing is development of multicomponent adsorption band in the range of 1000–1500 cm^{-1}. It can be assigned to disordered epoxy C—O—C (1220 cm^{-1}) and alkoxy C—O—C groups (1050 cm^{-1}) [31,37]. Additionally, it should be noted that after the high-temperature annealing at 650 °C FTIR spectrum demonstrates a strong adsorption in the range from 2000 to 5000 cm^{-1} (Fig. 3(b)) which is associated with adsorption of free charge carriers [32,38] and is in agreement with the considerable increase in electrical conductivity of the carbon film, that will be reported in Section 5. As a summary, it can be concluded that the main effect of thermal annealing treatment is dehydrogenation and transformation of hydrogenated sp^3 hybridized amorphous carbon into sp^2 hybridized carbon structural network. Significant contribution of oxygen related bonds after annealing is suggested to be due to the effect of oxidation by residual oxygen in the oven.

3.3. Raman spectroscopy

Obtained Raman spectra for as-deposited and annealed at 350, 550, and 650 °C samples #3 (see Table 1) are presented in Fig. 4. Spectra of as-deposited, and annealed at 350 °C samples have a strong photoluminescence background with weak Raman scattering features at 1350 cm^{-1} and 1590 cm^{-1} that can be assigned to D and G bands of amorphous carbon (Fig. 4(a)). After annealing at 550 and 650 °C the photoluminescence background vanished and well defined D- and G-bands can be seen now at 1350 cm^{-1} and 1590 cm^{-1} as well as corresponding 2D multiphonon band at 2700–2900 cm^{-1} (Fig. 4(a)). Such spectra are quite typical for defective graphitic structures [39,40].

Deconvolutions of the Raman spectra, using approach considered in papers [41], for samples annealed at 550 and 650 °C are presented in Fig. 4(b) and (c). The Raman spectra are very similar to ones of few layer wrinkled graphene (FLwG) [42] and demonstrate appearance of the bands at 1180 cm^{-1} (D* line), 1350 cm^{-1} (D line), 1450 cm^{-1} (D** line), 1590 cm^{-1} (G line) and 1610 cm^{-1} (D′ line). In paper [41] it was suggested that the bands D* and D** are the sum and difference of C=C stretching and C—H wagging modes of transpolyacetylene (alternating chain of sp^2 carbons with a single hydrogen bonded to carbon) in nanocrystalline diamond. However, in some papers [43,44] the D* peak has been attributed to sp^3 rich phase of disordered amorphous carbons and D** peak — to states in finite size graphitic crystals or due to C—H vibrations in hydrogenated carbons. In our case, the assumption proposed in paper [41] seems to be valid, since we study transformation of hydrogenated porous carbon into porous graphite and in the temperature range from 540 to 600 °C C—H bonds are broken, and hydrogen leaves the carbon material [45]. After annealing at 650 °C residual (sp^3) C—H bonds are observed in our FTIR spectra (Fig. 3(b)). Because I_D/I_G and $I_D/(I_G + I_D)$ for the samples annealed at 550 °C are 0.82 and 0.45, and for the samples annealed at 650 °C equal to 0.90 and 0.47, correspondingly, it can be concluded that the high-temperature annealing incorporates additional defects in the graphite plane.

4. Structure investigation and surface morphology

4.1. XRR

The film density, ρ_m, was determined using critical angle θ_C, at which X-ray wave is able to penetrate into the film. Snell's law gives:

$$\rho_m = \pi M_C \theta_C^2 / \lambda^2 N_A Z_C r_{el}, \quad (1)$$

where $r_{el} = e^2 / 4\pi\varepsilon_0 m_e c^2$ — is effective electron radius, N_A — is Avogadro constant, M_C — is carbon molar mass. Thickness of the thin film on the substrate can be determined using interference pattern of two reflected beams (from the film surface and film–substrate interface).

Fig. 5 demonstrates the dependence of X-ray refraction intensity vs. angle of incidence for both as deposited and annealed at 650 °C films. Critical angles for Si substrate and carbon film before and after thermal treatment have been detected from corresponding interference patterns.

Using thickness values and Eq. (1) the densities of the carbon films before annealing were estimated. From data presented in Table 3 we can conclude that as-deposited carbon films have low density (from 1.30 to 1.33 g/cm^3) which is increased a little after high-temperature

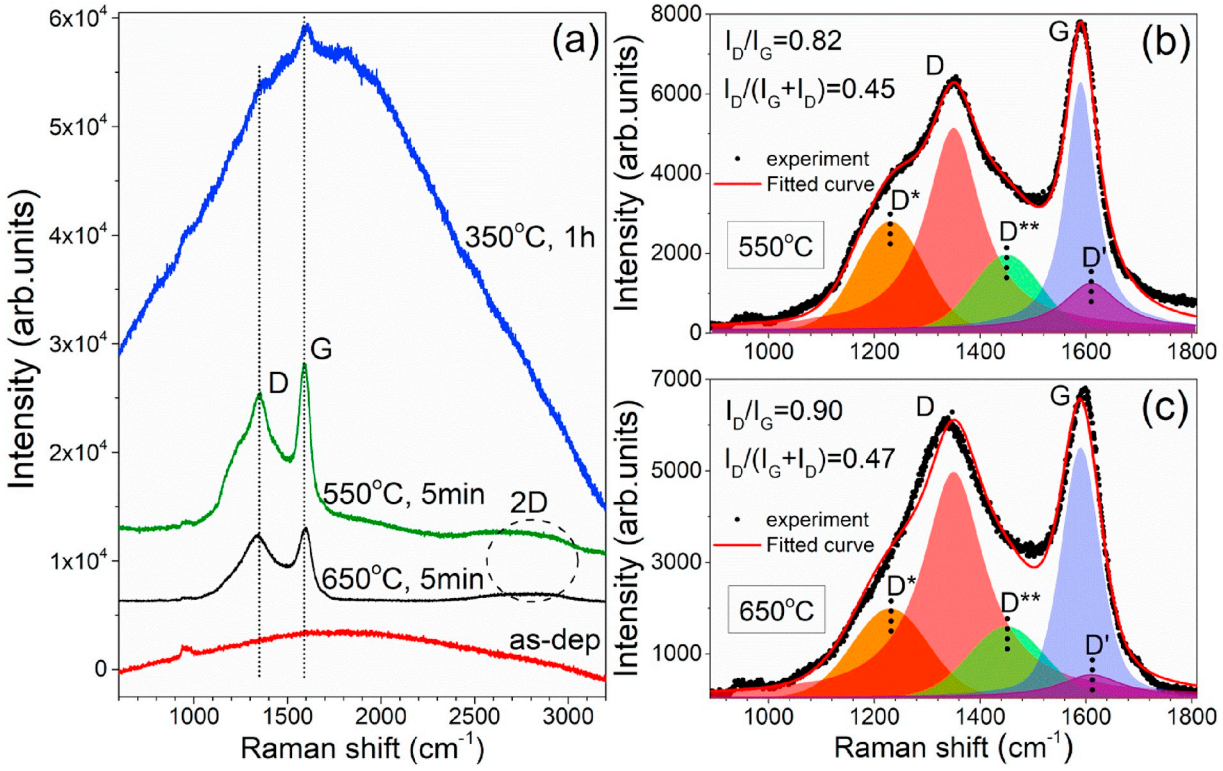

Fig. 4. Raman spectra for the sample #3 before and after annealing at 350, 550, and 650 °C (a). Deconvolution of the spectra for 550 (b) and 650 °C (c) annealing temperatures.

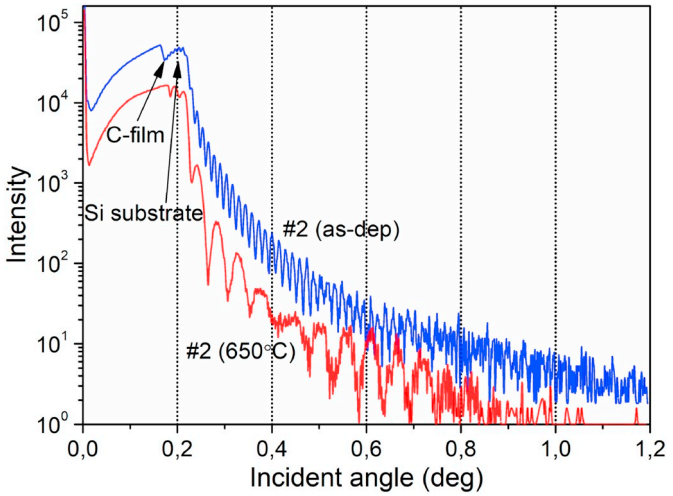

Fig. 5. XRR patterns obtained for the sample #2 before and after thermal annealing at 650 °C for 5 min.

annealing (up to 1.50 g/cm^3). Additionally after the annealing a surface roughness of the carbon films decreases. It should be noted that the thickness of the films after the high-temperature annealing is considerably decreased that is associated with the film burning by residual oxygen in annealing furnace.

Comparing the density of our carbon films with the value for tetrahedral amorphous carbon (ta-C: 3.26 g/cm^3 [18,46]) and graphite (2.26 g/cm^3 [19]) we can estimate porosity of the film Φ(%) using simple equation:

$$\Phi(\%) = [1 - (\rho_m/\rho_c)] \times 100\%, \quad (2)$$

where ρ_c is the density of reference material. Porosity of as-deposited films was calculated using the density of ta-C as reference, while for annealed film the density of graphite was used. Results presented in Table 3, show, that porosity of as-deposited films is about 59% and reduced down to 34% after annealing but it remains large enough.

Table 3
The parameters of the films, which were evaluated by the fitting of the experimental XRR curves.

Sample	Density of C layer, (g/cm^3)	Porosity of C layer, (%)	Thickness of C layer, (nm)	RMS Roughness of Si—C interface, (nm)	RMS Roughness of C-air interface, (nm)
#1	1.34	59	343	1.8	4.3
#1 annealed	1.48	35	41.5	0	2
#2	1.30	60	272	1.5	4
#2 annealed	1.5	34	36.5	0	2.1
#3	1.33	59	450	2.5	6.3
#3 annealed	1.5	34	78	0.5	3
#4	1.325	59	450	2.1	6.4
#4 annealed	1.5	34	93.5	0	3

4.2. AFM

Surface morphology of the films was investigated by AFM operated in tapping mode using ultra sharp silicon tip of 8 nm nominal apex radius. For minimization of the AFM tip effect, (overlapping of a tip shape and a real surface relief) a deconvolution of the surface maps was performed using the method of blind tip reconstruction [47]. Topography maps and corresponding surface profiles of the carbon films before and after annealing are illustrated in Fig. 6. Surface morphology of as-deposited film is characterized by RSM roughness of about 3.3 nm and exhibits nanoscale granular topography that is quite typical for growth morphology of amorphous films deposited on “cold surface” [48]. It is important to point out that the surface of the film contains a large amount of holes/pores with size of few tens of nanometers (black

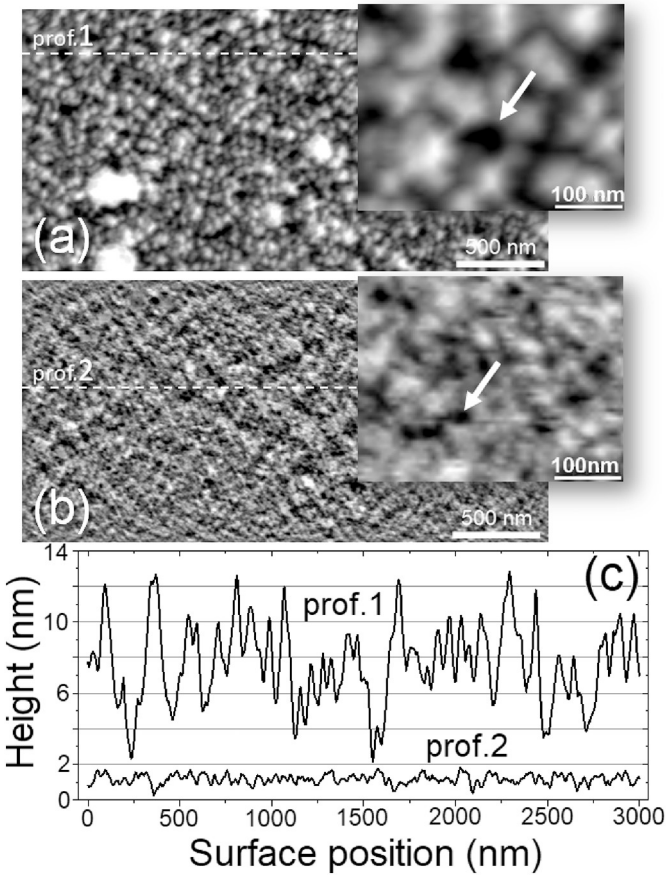

Fig. 6. Deconvolution of AFM images for as-deposited (a) and annealed at 650 °C (b) carbon films (Sample #3). Corresponding cross-section profiles of surface relief are shown in (c). Pores indicated by arrows in enlarged fragments of corresponding images.

regions pointed by arrow in inset of Fig. 6(a, b)). It is believed that highly inhomogeneous surface morphology is related to low density of the film. The main effect of the annealing is a drastic decrease of the surface roughness down to about 0.6 nm (Fig. 6(c)). It is reasonable to suggest that surface smoothening is a combined effect of thermally activated densification and chemical etching of the surface by residual oxygen available in the furnace.

5. Electrical properties

Resistivity data for samples #1, #2, #3 and #4, measured by four point probe method, before and after annealing at 350, 550 and 650 °C are presented in Fig. 7. Resistivity of the samples annealed at 650 °C decreases by 5 orders of magnitude as compared to as-deposited samples, and reaches the value of 5×10^3–1×10^4 Ω/cm. I-V characteristics for all samples before and after annealing are presented in Fig. 8. Starting from 550 °C, the dependences become Ohmic. Resistance of samples #4 and #2 decreases from 5×10^{12} Ω to 2×10^7 Ω. It should be mentioned, that these two samples were prepared with minimum plasma power, and have lower densities (higher porosity) after deposition, compared to samples #3 and #1. Thus, after high-temperature annealing, we have obtained porous conducting films suitable for fabrication of gas sensors based on the resistivity response.

6. Sensor properties

The response on chemical ambient was examined by measurement of electric current between a contacts pair at fixed signal level (1 V).

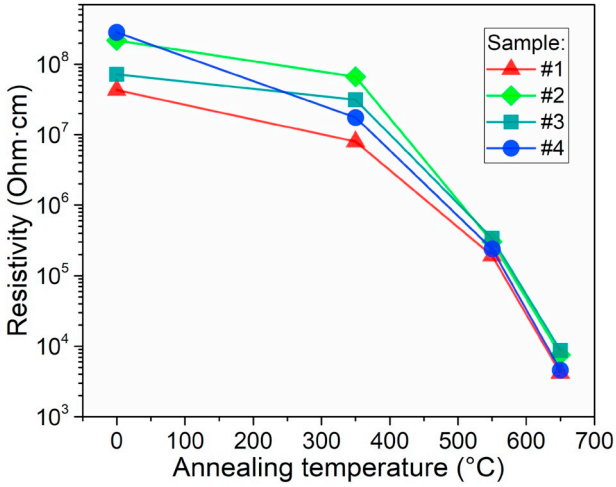

Fig. 7. Carbon films resistivity vs. annealing temperature.

Results for such analytes as ammonia (NH_3), acetone ($(CH_3)_2CO$), ethanol (C_2H_5OH) and water vapor are presented in Fig. 9. The relative resistance changes ($\Delta R/R_0$) were found to be 2–3.5% for $(CH_3)_2CO$, 5–6% for C_2H_5OH, 5–6.5% for water vapor and 12–19% for NH_3. Ammonia, acetone and ethanol increase the resistance of the carbon film with maximum sensitivity to ammonia, whereas water vapor results in the decrease of the carbon film resistance. It can be assumed that ammonia, acetone and ethanol are strong electron-donating or withdrawing molecules [49], while water molecule decomposing into OH^- and H^+ probably extracts electron from carbon. In the first case the resistance becomes higher, in the second — lower.

Indeed adsorption of organic vapors on graphite surface occurs through the dissociation of the organic molecules to H^+ or OH^- ions to form many different intermediate states. The final reactions of ethanol and acetone with adsorbed oxygen species on carbon surface can be described in the following form, as it was proposed for graphene oxide layer [50]:

$$C_2H_5OH(ads) + 6O^-(ads) \rightarrow 2CO_2 + 3H_2O + 6e^-, \quad (3)$$

$$(CH_3)_2CO(ads) + 8O^-(ads) \rightarrow 3CO_2(g) + 3H_2O(g) + 8e^-. \quad (4)$$

The similar approach can be used to explain ammonia reaction on surface of graphite which contains adsorbed oxygen [51]:

$$2NH_3(ads) + 3O^-(ads) \rightarrow N_2(g) + 3H_2O(g) + 3e^-. \quad (5)$$

The sensing mechanism of ethanol, acetone and ammonia is based on the fact that the electrons from the chemical reactions mentioned above transfer to the graphite, which results in hole depletion of p-type oxidized graphite, thereby, increasing the resistance of the porous graphite film. It should be noted that at room temperature a saturation of resistance of the porous graphite film during introduction of the gases into chamber and desorption of the gases is observed in considerably less time scale than in the case of reduced graphene oxide (rGO) film fabricated by spray pyrolysis method [52] that can be explained with adsorption of the gases mainly on the surface of the pores of the graphite film. In case of rGO film fabricated by spray pyrolysis method the gases probably penetrate into interlayer area (between flakes) that considerably slows down time of the reactions with the material and can lead to the increase of the film resistance by increasing the distance between flakes.

The former effect is especially noticeable for water vapor. In the case of rGO film fabricated by spray pyrolysis method the effect of water vapor on the film consists in incorporation of water molecules into interlayer space between GO flakes which leads to a considerable increase of the resistance at adsorption and small recovering effect at air blowing at room temperature [52]. In the case of the porous

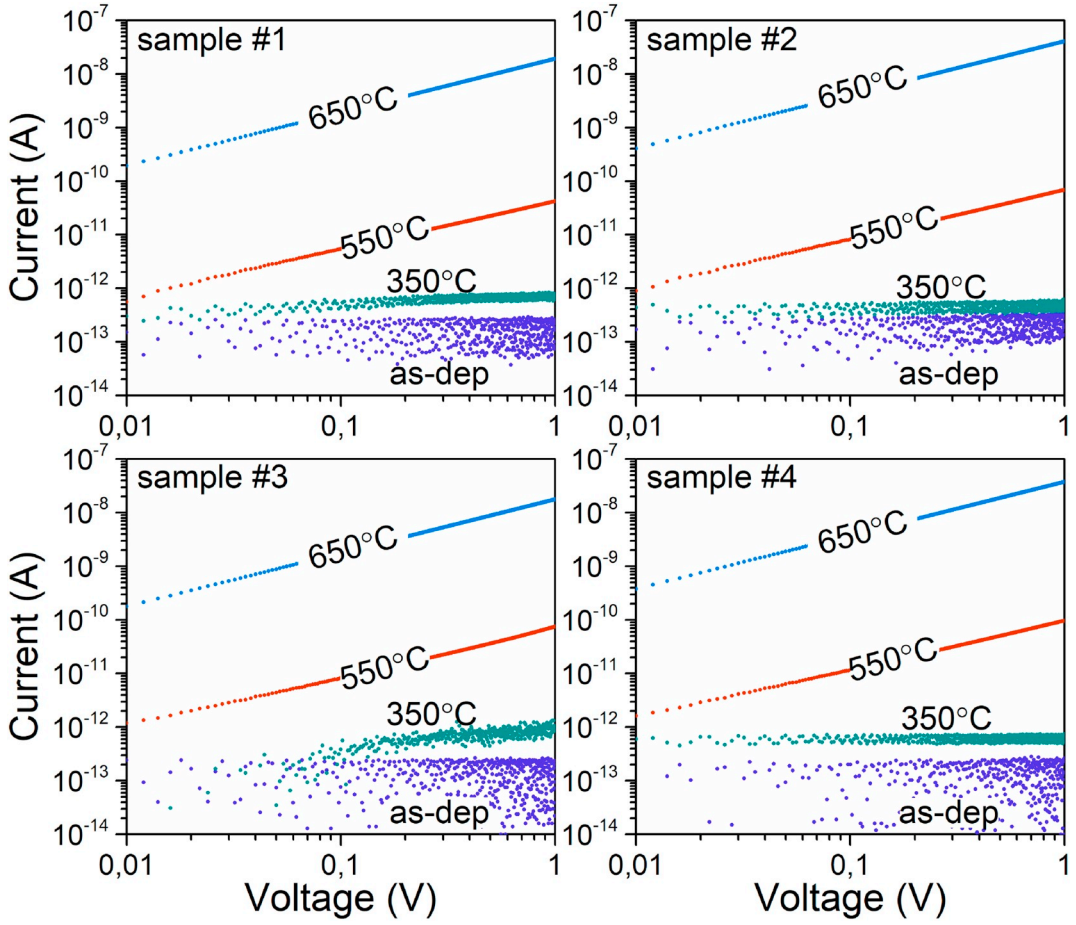

Fig. 8. The I-V characteristics for as-deposited and post annealed (at 350, 550, 650 °C) carbon films.

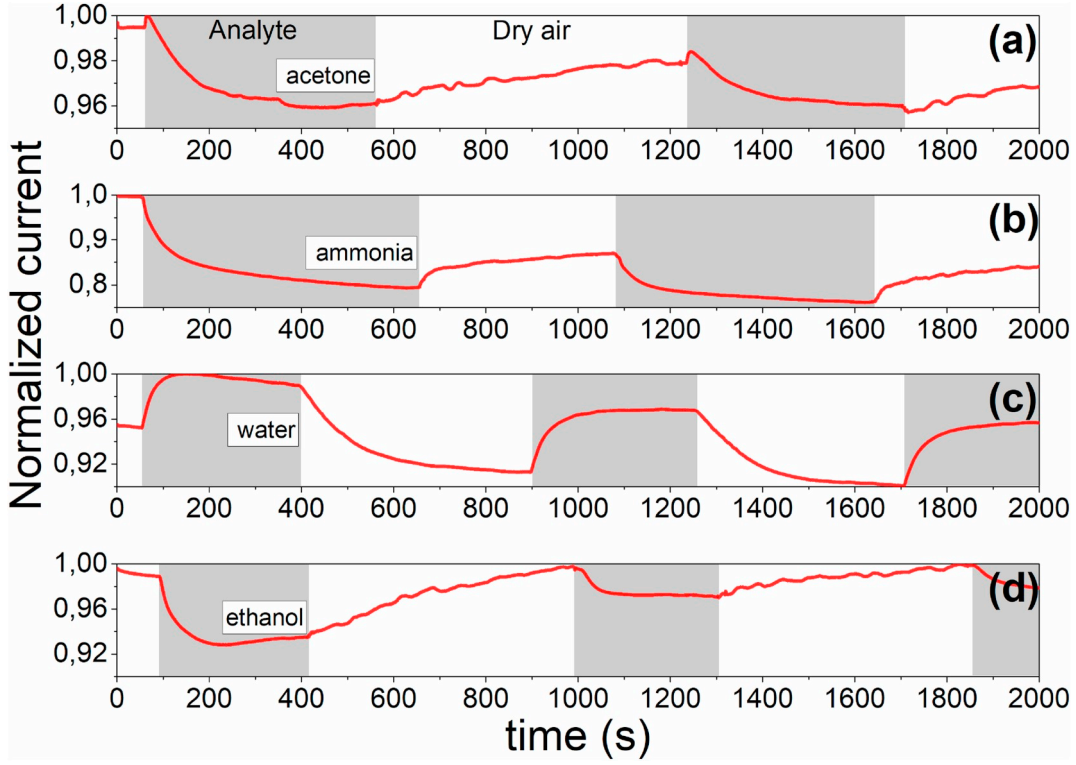

Fig. 9. Time dependences of normalized current (for 1 V applied voltage) for #2 sample, measured under (a) acetone, (b) ammonia, (c) water vapor and (d) ethanol vapor.

graphite film we observe a strong decrease of the film resistance at adsorption with good recovering effect at air blowing and a slight effect of a gradual increase of resistance during adsorption/desorption processes (Fig. 9(c)). From last observations we can conclude that incorporation of water molecules into amorphous porous graphitized carbon film does not lead to exfoliation of the graphitic skeleton due to its higher density as compared with GO obtained by spray pyrolysis method. At the same time water molecules dissociate at defects of carbon skeleton with formation of hydroxyl groups and protons. The protons take part in proton transport of the charge which decreases resistance of the material. Indeed in paper [53] a decrease of resistance at water vapor adsorption in porous materials was explained by decomposition of water molecules at porous surface to OH^- and H^+, and proton transport (at low water vapor concentration) or H_3O^+ ion transport (at existence of water monolayer). An additional constant increase of resistance of the porous carbon film can be associated with introduction of the water molecules into interlayer region of the graphite film that decreases the electrical contact between the layers. It is interesting that similar phenomenon was observed in paper [54] for GO films synthesized by chemical exfoliation for high level of humidity. Probably the last method of synthesis forms GO film with higher density in comparison with spray pyrolysis method.

It should be noted that gradual increasing of the film resistance is observed also for acetone and ammonia adsorption that can be related to decomposition reaction of the analytes with water formation which can penetrate into interlayer space of the films.

7. Conclusions

The new method of formation of porous graphite-like thin films by RF magnetron plasma enhanced chemical vapor deposition from argon-methane gas mixture followed by annealing at 650 °C, is suggested. The complex of diagnostic methods, consisting of XPS/XES, FTIR, XDR, AFM, Raman spectroscopy and electrical measurements were employed to examine chemical, structural and electrical properties before and after high-temperature annealing. The structure of as-deposited carbon films was found to be amorphous with domination of sp^3 coordinated carbon atoms. Growth morphology of the films is highly porous (calculated porosity is of about 59%) with very low electrical conductivity. Annealing of the film in nitrogen atmosphere at 650 °C results in "graphitization" of the film, the decrease of porosity of the film (down to about 35%) and the strong decrease of electrical resistance (up to 5 orders of magnitude as compared to as-deposited material). Resistivity of such films exhibited good gas sensitivity particularly to ammonia and water vapor. The gas sensing properties of the carbon film was shown to be very similar to that of reduced graphene oxide.

Acknowledgements

Authors acknowledge Science & Technology Center in Ukraine for partial support (Project #6362).

References

[1] J. Robertson, Hard amorphous (diamond-like) carbons, Prog. Solid State Chem. 21 (1991) 199–333, https://doi.org/10.1016/0079-6786(91)90002-h.
[2] J. Robertson, Diamond-like amorphous carbon, Materials Science and Engineering: R: Reports 37 (2002) 129–281, https://doi.org/10.1016/s0927-796x(02)00005-0.
[3] S.I. Kim, B.B. Sahu, S.E. Kim, A. Ali, E.H. Choi, J.G. Han, Controlling conductivity of carbon film for L-929 cell biocompatibility using magnetron sputtering plasmas, J. Mater. Chem. B 3 (2015) 3267–3278, https://doi.org/10.1039/c4tb01397b.
[4] I. Matos, M. Bernardo, I. Fonseca, Porous carbon: a versatile material for catalysis, Catal. Today 285 (2017) 194–203, https://doi.org/10.1016/j.cattod.2017.01.039.
[5] L. Wang, X. Hu, Recent advances in porous carbon materials for electrochemical energy storage, Chemistry-An Asian Journal 13 (2018) 1518–1529, https://doi.org/10.1002/asia.201800553.
[6] Y. Nishi, M. Inagaki, Gas adsorption/desorption isotherm for pore structure characterization, Materials Science and Engineering of Carbon, 2016, pp. 227–247, , https://doi.org/10.1016/b978-0-12-805256-3.00011-8.
[7] W. Dai, S.J. Kim, W.-K. Seong, S.H. Kim, K.-R. Lee, H.-Y. Kim, et al., Porous carbon nanoparticle networks with tunable absorbability, Sci. Rep. 3 (2013), https://doi.org/10.1038/srep02524.
[8] N.A. Travlou, M. Seredych, E. Rodríguez-Castellón, T.J. Bandosz, Activated carbon-based gas sensors: effects of surface features on the sensing mechanism, J. Mater. Chem. A 3 (2015) 3821–3831, https://doi.org/10.1039/c4ta06161f.
[9] G. Che, B.B. Lakshmi, E.R. Fisher, C.R. Martin, Carbon nanotubule membranes for electrochemical energy storage and production, Nature 393 (1998) 346–349, https://doi.org/10.1038/30694.
[10] J. Schwan, S. Ulrich, H. Roth, H. Ehrhardt, S.R.P. Silva, J. Robertson, et al., Tetrahedral amorphous carbon films prepared by magnetron sputtering and dc ion plating, J. Appl. Phys. 79 (1996) 1416–1422, https://doi.org/10.1063/1.360979.
[11] F. Qian, R.K. Singh, S.K. Dutta, P.P. Pronko, Laser deposition of diamondlike carbon films at high intensities, Appl. Phys. Lett. 67 (1995) 3120–3122, https://doi.org/10.1063/1.114853.
[12] M. Acharya, H.C. Foley, Spray-coating of nanoporous carbon membranes for air separation, J. Membr. Sci. 161 (1999) 1–5, https://doi.org/10.1016/s0376-7388(99)00173-8.
[13] M.B. Shiflett, H.C. Foley, On the preparation of supported nanoporous carbon membranes, J. Membr. Sci. 179 (2000) 275–282, https://doi.org/10.1016/s0376-7388(00)00513-5.
[14] E.N. Kalabukhova, S.N. Lukin, D.V. Savchenko, B.D. Shanina, A.V. Vasin, V.S. Lysenko, et al., EPR study of carbon and silicon related defects in carbon-rich hydrogenated amorphous silicon-carbon films, Phys. Rev. B 81 (2010), https://doi.org/10.1103/physrevb.81.155319.
[15] A. Vasin, A. Rusavsky, A. Nazarov, V. Lysenko, P. Lytvyn, V. Strelchuk, et al., Identification of nanoscale structure and morphology reconstruction in oxidized a-SiC:H thin films, Appl. Surf. Sci. 260 (2012) 73–76, https://doi.org/10.1016/j.apsusc.2012.04.016.
[16] G. Capote, F.L. Freire, L.G. Jacobsohn, G. Mariotto, Amorphous hydrogenated carbon films deposited by PECVD in methane atmospheres highly diluted in argon: effect of the substrate temperature, Diam. Relat. Mater. 13 (2004) 1454–1458, https://doi.org/10.1016/j.diamond.2003.11.030.
[17] Hüfner Stefan, Photoelectron Spectroscopy: Principles and Applications, 3rd ed., Springer, Berlin, 2003.
[18] O. Khyzhun, XPS, XES, and XAS studies of the electronic structure of substoichiometric cubic TaCx and hexagonal Ta_2C_y carbides, J. Alloys Compd. 259 (1997) 47–58, https://doi.org/10.1016/s0925-8388(97)00098-4.
[19] J.C. Rivière, S. Myhra, Handbook of Surface and Interface Analysis: Methods for Problem-Solving, 2nd ed., CRC Press, Boca Raton, 2009.
[20] O. Khyzhun, T. Strunskus, W. Grünert, C. Wöll, Valence band electronic structure of V_2O_5 as determined by resonant soft X-ray emission spectroscopy, J. Electron Spectrosc. Relat. Phenom. 149 (2005) 45–50, https://doi.org/10.1016/j.elspec.2005.07.002.
[21] D.K. Schroder, Semiconductor Material and Device Characterization, 3rd ed., John Wiley & Sons, Hoboken, NJ, 2006, p. 779.
[22] D. Briggs, M.P. Seah (Eds.), Practical Surface Analysis. Vol. 1. Auger and X-ray Photoelectron Spectroscopy, 2nd ed., John Wiley and Sons, Chichester, 1990.
[23] J.F. Morar, F.J. Himpsel, G. Hollinger, J.L. Jordon, G. Hughes, F.R. Mcfeely, C1s excitation studies of diamond (111). II. Unoccupied surface states, Phys. Rev. B 33 (1986) 1346–1349, https://doi.org/10.1103/physrevb.33.1346.
[24] O. Khyzhun, E. Zhurakovsky, A. Sinelnichenko, V. Kolyagin, Electronic structure of tantalum subcarbides studied by XPS, XES, and XAS methods, J. Electron Spectrosc. Relat. Phenom. 82 (1996) 179–192, https://doi.org/10.1016/s0368-2048(96)03057-5.
[25] J. Leiro, M. Heinonen, T. Laiho, I. Batirev, Core-level XPS spectra of fullerene, highly oriented pyrolitic graphite, and glassy carbon, J. Electron Spectrosc. Relat. Phenom. 128 (2003) 205–213, https://doi.org/10.1016/s0368-2048(02)00284-0.
[26] A.J. Barlow, S. Popescu, K. Artyushkova, O. Scott, N. Sano, J. Hedley, et al., Chemically specific identification of carbon in XPS imaging using Multivariate Auger Feature Imaging (MAFI), Carbon 107 (2016) 190–197, https://doi.org/10.1016/j.carbon.2016.05.073.
[27] D.M. Poirier, J.H. Weaver, Carbon (as graphite, buckminsterfullerene, and diamond) by XPS, Surface Science Spectra 2 (1993) 232–241, https://doi.org/10.1116/1.1247704.
[28] J. Díaz, G. Paolicelli, S. Ferrer, F. Comin, Separation of the sp^3 and sp^2 components in the C 1s photoemission spectra of amorphous carbon films, Phys. Rev. B 54 (1996) 8064–8069, https://doi.org/10.1103/physrevb.54.8064.
[29] R.M. Dey, M. Pandey, D. Bhattacharyya, D.S. Patil, S.K. Kulkarni, Diamond like carbon coatings deposited by microwave plasma CVD: XPS and ellipsometric studies, Bull. Mater. Sci. 30 (2007) 541–546, https://doi.org/10.1007/s12034-007-0084-8.
[30] J. Zhao, J. Wang, J. Zhi, Z. Zhang, Preparation of grain size controlled boron-doped diamond thin films and their applications in selective detection of glucose in basic solutions, Science China Chem. 53 (2010) 1378–1384, https://doi.org/10.1007/s11426-010-3099-8.
[31] A. Kurdyumov, V. Britun, O. Khyzhun, Y. Zaulychnyy, V. Bekenev, V. Dymarchuk, et al., Structure of the dense amorphous carbon phase synthesized in a mixture with diamond as a result of shock compression of carbon black, Diam. Relat. Mater. 20 (2011) 974–979, https://doi.org/10.1016/j.diamond.2011.05.019.
[32] K. Endo, S. Koizumi, T. Otsuka, M. Suhara, T. Morohasi, E.Z. Kurmaev, et al., Analysis of XPS and XES of diamond and graphite by DFT calculations using model molecules, J. Comput. Chem. 22 (2000) 102–108, https://doi.org/10.1002/1096-987x(20010115)22:1<102::aid-jcc10>3.0.co;2-f.
[33] B.H. Stuart, Infrared Spectroscopy: Fundamentals and Applications, J. Wiley, Chichester, West Sussex, England, 2004, p. 244.

[34] P. Kumar, A.K. Singh, S. Hussain, K.N. Hui, K.S. Hui, J. Eom, et al., Graphene: synthesis, properties and application in transparent electronic devices, Reviews in Advanced Sciences and Engineering 2 (2013) 238–258, https://doi.org/10.1166/rase.2013.1043.
[35] Leila Shahriary, A.A. Athawale, Graphene oxide synthesized by using modified hummers approach, Int. J. Energy Environ. Eng. 2 (2014) 58–63.
[36] X.B. Yan, T. Xu, S.R. Yang, H.W. Liu, Q.J. Xue, Characterization of hydrogenated diamond-like carbon films electrochemically deposited on a silicon substrate, J. Phys. D. Appl. Phys. 37 (2004) 2416–2424, https://doi.org/10.1088/0022-3727/37/17/012.
[37] H. Wang, Y.H. Hu, Effect of oxygen content on structures of graphite oxides, Ind. Eng. Chem. Res. 50 (2011) 6132–6137, https://doi.org/10.1021/ie102572q.
[38] D.A. Panayotov, S.P. Burrows, J.R. Morris, Infrared spectroscopic studies of conduction band and trapped electrons in UV-photoexcited, H-atom n-doped, and thermally reduced TiO_2, J. Phys. Chem. C 116 (2012) 4535–4544, https://doi.org/10.1021/jp2053103.
[39] A. Cuesta, P. Dhamelincourt, J. Laureyns, A. Martínez-Alonso, J.M.D. Tascón, Comparative performance of X-ray diffraction and Raman microprobe techniques for the study of carbon materials, J. Mater. Chem. 8 (1998) 2875–2879, https://doi.org/10.1039/a805841e.
[40] S. Claramunt, A. Varea, D. López-Díaz, M.M. Velázquez, A. Cornet, A. Cirera, The importance of interbands on the interpretation of the Raman spectrum of graphene oxide, J. Phys. Chem. C 119 (2015) 10123–10129, https://doi.org/10.1021/acs.jpcc.5b01590.
[41] A.C. Ferrari, J. Robertson, Origin of the1150-cm^{-1} Raman mode in nanocrystalline diamond, Phys. Rev. B 63 (2001), https://doi.org/10.1103/physrevb.63.121405.
[42] A. Kaniyoor, S. Ramaprabhu, A Raman spectroscopic investigation of graphite oxide derived graphene, AIP Adv. 2 (2012) 032183, , https://doi.org/10.1063/1.4756995.
[43] J. Schwan, S. Ulrich, V. Batori, H. Ehrhardt, S.R.P. Silva, Raman spectroscopy on amorphous carbon films, J. Appl. Phys. 80 (1996) 440–447, https://doi.org/10.1063/1.362745.
[44] R.E. Shroder, R.J. Nemanich, J.T. Glass, Analysis of the composite structures in diamond thin films by Raman spectroscopy, Phys. Rev. B 41 (1990) 3738–3745, https://doi.org/10.1103/physrevb.41.3738.
[45] S. Peter, M. Günther, F. Richter, A comparative analysis of a-C:H films deposited from five hydrocarbons by thermal desorption spectroscopy, Vacuum 86 (2012) 667–671, https://doi.org/10.1016/j.vacuum.2011.07.037.
[46] A. Libassi, A.C. Ferrari, V. Stolojan, B.K. Tanner, J. Robertson, L.M. Brown, Density and sp^3 content in diamond-like carbon films by X-ray reflectivity and electron energy loss spectroscopy, MRS Proc. 593 (1999), https://doi.org/10.1557/proc-593-293.
[47] F. Tian, X. Qian, J. Villarrubia, Blind estimation of general tip shape in AFM imaging, Ultramicroscopy 109 (2008) 44–53, https://doi.org/10.1016/j.ultramic.2008.08.002.
[48] M. Raible, S.J. Linz, P. Hänggi, Amorphous thin film growth: effects of density inhomogeneities, Phys. Rev. E 64 (2001), https://doi.org/10.1103/physreve.64.031506.
[49] V.A. Skryshevsky, Y.S. Milovanov, I.V. Gavrilchenko, S.I. Tiagulskyi, A.V. Rusavsky, V.S. Lysenko, et al., Impedance spectroscopy of single graphene layer at gas adsorption, Phys. Status Solidi A 212 (2015) 1941–1945, https://doi.org/10.1002/pssa.201532101.
[50] M. Gautam, A.H. Jayatissa, Detection of organic vapors by graphene films functionalized with metallic nanoparticles, J. Appl. Phys. 112 (2012) 114326, , https://doi.org/10.1063/1.4768724.
[51] M. Gautam, A.H. Jayatissa, Ammonia gas sensing behavior of graphene surface decorated with gold nanoparticles, Solid State Electron. 78 (2012) 159–165, https://doi.org/10.1016/j.sse.2012.05.059.
[52] O.M. Slobodian, et al., Reduced graphene oxide obtained using the spray pyrolysis technique for gas sensing, Semiconductor Physics, Quantum Electronics & Optoelectronics 22 (2019) 98–103, https://doi.org/10.15407/spqeo22.01.098.
[53] J.H. Anderson, G.A. Parks, Electrical conductivity of silica gel in the presence of adsorbed water, J. Phys. Chem. 72 (1968) 3662–3668, https://doi.org/10.1021/j100856a051.
[54] G. Naik, S. Krishnaswamy, Room-temperature humidity sensing using graphene oxide thin films, Graphene 05 (2016) 1–13, https://doi.org/10.4236/graphene.2016.51001.